Published OnlineFirst May 15, 2018; DOI: 10.1158/2326-6066.CIR-17-0408

Research Article

Cancer Immunology Research

Subcellular Localization of Antigen in Keratinocytes Dictates Delivery of CD4$^+$ T-cell Help for the CTL Response upon Therapeutic DNA Vaccination into the Skin

Nikolina Bąbała[1], Astrid Bovens[1], Evert de Vries[1], Victoria Iglesias-Guimarais[1], Tomasz Ahrends[1], Matthew F. Krummel[2], Jannie Borst[1], and Adriaan D. Bins[1]

Abstract

In a mouse model of therapeutic DNA vaccination, we studied how the subcellular localization of vaccine protein impacts antigen delivery to professional antigen-presenting cells and efficiency of CTL priming. Cytosolic, membrane-bound, nuclear, and secretory versions of ZsGreen fluorescent protein, conjugated to MHC class I and II ovalbumin (OVA) epitopes, were expressed in keratinocytes by DNA vaccination into the skin. ZsGreen-OVA versions reached B cells in the skin-draining lymph node (dLN) that proved irrelevant for CTL priming. ZsGreen-OVA versions were also actively transported to the dLN by dendritic cells (DC). In the dLN, vaccine proteins localized to classical (c)DCs of the migratory XCR1$^+$ and XCR$^-$ subtypes, and—to a lesser extent—to LN-resident cDCs. Secretory ZsGreen-OVA induced the best antitumor CTL response, even though its delivery to cDCs in the dLN was significantly less efficient than for other vaccine proteins. Secretory ZsGreen-OVA protein proved superior in CTL priming, because it led to *in vivo* engagement of antigen-loaded XCR1$^+$, but not XCR1$^-$, cDCs. Secretory ZsGreen-OVA also maximally solicited CD4$^+$ T-cell help. The suboptimal CTL response to the other ZsGreen-OVA versions was improved by engaging costimulatory receptor CD27, which mimics CD4$^+$ T-cell help. Thus, in therapeutic DNA vaccination into the skin, mere inclusion of helper epitopes does not ensure delivery of CD4$^+$ T-cell help for the CTL response. Targeting of the vaccine protein to the secretory route of keratinocytes is required to engage XCR1$^+$ cDC and CD4$^+$ T-cell help and thus to promote CTL priming. *Cancer Immunol Res; 6(7); 835–47. ©2018 AACR.*

Introduction

Therapeutic vaccination aims to elicit CTL responses against cancer or infectious disease. Despite its promise, this approach is not yet predictably effective and requires rational optimization (1). Requirements for effective vaccine design begin with selection of vaccine antigens, based upon the molecular characterization of the cancer or infectious agent. Then, vaccine formulation and application must take into account the molecular and cellular requirements for CTL priming. For example, the vaccine antigen should be delivered to adequate professional antigen-presenting cell (pAPC; ref. 2). Dendritic cells (DCs) are considered the key pAPC type to elicit a CTL response, but a role for macrophages and/or B cells is not excluded (3, 4). The vaccine should also activate antigen-presenting DCs, because in their steady state, these cells maintain T-cell tolerance (2). DCs are subdivided into two major lineages, plasmacytoid (p)DCs and myeloid DCs. The latter are also called classical (c)DCs. Among cDCs, XCR1$^+$ and CD11b$^+$ lineages are discerned, each with a migratory and lymph node (LN)–resident subset (5).

DCs sense micro-organisms and "danger" by cell-surface and intracellular receptors (6, 7). When activated, they become optimized for T-cell priming through upregulation of antigen-presenting functions, costimulatory ligands, and cytokines (1, 2). CD4$^+$ T-cell help can also promote CTL priming (8, 9), so therapeutic vaccines should include MHC class II–binding peptides (helper epitopes) next to MHC class I–binding peptides (CTL epitopes; refs. 1, 10). Intravital imaging in mice revealed that, after virus infection, antigen-specific CD4$^+$ and CD8$^+$ T cells are initially activated by distinct (migratory) cDC subsets in the LN or spleen. In a second stage of priming, they come together on the same LN-resident XCR1$^+$ cDC (11–13). In this cellular scenario, the CD4$^+$ T cell delivers—via the cDC—"help" signals to the CD8$^+$ T cell that promote CTL clonal expansion, effector and memory differentiation (8, 9, 11, 12).

Vaccines are generally injected into the skin, because antigen can easily reach draining lymph nodes (dLN) from this site, either via active transport by skin-resident pAPC or by passive draining from the dermis via lymph vessels (14). In DNA vaccination,

[1]Division of Tumor Biology and Immunology, The Netherlands Cancer Institute-Antoni van Leeuwenhoek, Amsterdam, the Netherlands. [2]Department of Pathology, University of California San Francisco, San Francisco, California.

Note: Supplementary data for this article are available at Cancer Immunology Research Online (http://cancerimmunolres.aacrjournals.org/).

J. Borst and A.D. Bins contributed equally to this article.

Current address for A.D. Bins: Department of Medical Oncology, Academic Medical Center, University of Amsterdam, Amsterdam, the Netherlands.

Corresponding Author: Jannie Borst, Netherlands Cancer Institute, Plesmanlaan 121, 1066 CX Amsterdam, the Netherlands. Phone: 31205122056; Fax: 31205122057; E-mail: j.borst@nki.nl

doi: 10.1158/2326-6066.CIR-17-0408

Published OnlineFirst May 15, 2018; DOI: 10.1158/2326-6066.CIR-17-0408

protein is expressed in transfected cells before it relocates to the relevant pAPCs. The cell type transfected with the vaccine DNA and the nature of the expressed protein likely impact antigen delivery to pAPCs and deserve systematic examination. The DNA vaccination strategy used in this study effectively raises CTL responses in mice and monkeys (15–17). In this approach, naked plasmid (p)DNA is "tattooed" into the epidermis, resulting in transient transfection of keratinocytes (16). Inclusion of helper epitopes in the DNA vaccine increases its potency in CTL priming (18). In the current study, we used a vaccine comprising helper and CTL epitopes linked to the fluorescent protein ZsGreen (19), to examine vaccine protein delivery to pAPCs. We tested cytosolic, membrane-bound, nuclear, and secretory forms of this vaccine protein, to examine the impact of its subcellular localization in transfected keratinocytes on antigen routing and immunogenicity.

We found that the magnitude of the CTL response was dictated by the subcellular localization of the vaccine protein in keratinocytes. Inclusion of helper epitopes in the vaccine did not ensure delivery of $CD4^+$ T-cell help, which is essential for CTL responsiveness to an implanted tumor. Vaccination with the secretory protein led to superior engagement of antigen-presenting migratory and LN-resident $XCR1^+$ cDCs, delivery of $CD4^+$ T-cell help, and optimal CTL priming. After vaccination with membrane-bound protein, antigen was more efficiently loaded into cDCs, but these cDCs did not become activated and were deficient in soliciting $CD4^+$ T-cell help, and they were therefore unable to prime $CD8^+$ T cells. Thus, not the quantity, but the quality, of antigen delivery to cross-presenting cDCs dictates delivery of $CD4^+$ T-cell help for the CTL response.

Materials and Methods

Mice

Wild-type C57BL/6JRj mice (Janvier Laboratories) and OT-I mice (C57BL/6-Tg(TcraTcrb)1100Mjb/J) on a C57BL/6JRj background were maintained in individually ventilated cages (Innovive). Experiments were performed with gender- and age-matched mice (8–12 weeks), according to national and institutional guidelines.

DNA constructs

The cDNA encoding cytosolic ZsGreen (Evrogen; ref. 19) was inserted into the pCAGGs plasmid (Addgene), using Mlu1 and Not1 restriction sites. A sequence encoding the chicken OVA fragment GSAESLK ISQAVHAAHAEINEAGR EVSGLEQLE SIINFEKL containing $OVA_{257\text{-}264}$ (SIINFEKL) and $OVA_{323\text{-}339}$ (ISQAVHAAHAEINEAGR) peptides was added at the C-terminus by PCR-based cloning. Nuclear, membrane-bound, and secretory versions of the cytoplasmic ZsGreen were generated by PCR-based addition of, respectively, an SV40 nuclear localization signal (NLS), a combined palmitoylation/myristoylation (PAM) signal (20), or the SLURP-1 signal peptide (SP) to the N-terminus of ZsGreenOVA, using the following forward primers in combination with M13 reverse primer: for NLS (MGPKKKRKV): acgcgtgccaccatggggcccaagaagaagaggaaagtccacgtgcagtccaagcacggcctgaccaaggag, for PAM (MGCTVSTQ): aataatacgcgtgccaccatgggctgtaccgtgtctacacagggcagcgacgtgcagagcaagcacggcc, for SP (MTLRWAMWLLLLAAWSMGYGEA): acgcgtgccaccatggtgtacacatccggaatgactctcaggtgggctatgtggctgctcttgctggccgcctggtccatgggatatggtgaagcagacctgcagggggatgatgtgcagtccaagcacggc. PCR products were ligated in pCAGGs after restriction with Mlu1 and Not1, and plasmid was transformed in DH5α *E. coli* for production.

Analysis of the subcellular localization of ZsGreen variants

HeLa cells (unknown origin, not reauthenticated) and short-term cultured immortalized keratinocytes (mTIC) from the original laboratory (21) were cultured in DMEM with 8% FBS and transfected using Fugene (Roche Applied Science) or Lipofectamine (Thermo Fisher Scientific), respectively. For microscopy, mTIC cells were grown and transfected on glass coverslips, washed in PBS, fixed with 4% paraformaldehyde in PBS, and permeabilized with 0.1% Triton X-100 in PBS. Blocking was performed in PBS with 1% BSA. Cells were stained with rabbit mAb to GRP78 (BIP) (ab21685, Abcam), followed by Alexa Fluor 568–conjugated anti-IgG, washed with PBS, counterstained with DAPI, and mounted with Vectashield (Vector labs). Images were acquired by sequential scanning using an inverted Leica SP5 confocal laser-scanning microscope (CLSM) equipped with 63 × 1.4 NA oil objective. To determine secretion of ZsGreen-OVA, supernatant medium of transfected HeLa cells was centrifuged at 100.000 × *g* for 30 minutes in an Airfuge (Beckman Coulter), and cells were lysed in 10 mmol/L Tris–HCl pH 7.8, 150 mmol/L NaCl, 1% Nonidet P-40, and protease inhibitors. Lysates were clarified by centrifugation for 15 minutes at 14.000 × *g* and ZsGreen fluorescence in supernatants and lysates was measured in a Tecan Infinite 200 plate reader with GFP fluorescence measuring mode.

Gene gun transfection and intravital microscopy of the pinna

The epidermis of the ear was transfected using a homemade gene gun. Gold bullets from BIO-RAD were coated with DNA according to their Helios gene gun protocol, with 1 mg/mL protamine (22) instead of spermidine. Bullets were shot in the dorsum of the pinna using a pressure of 400 psi, at a distance of 5 cm. For intravital microscopy, mice were anesthetized and fixed in a custom-made "helmet" that enabled positioning of a coverslip over both ears. The helmet was mounted on a 37°C plate underneath the objective of a 2-photon microscopy setup (23), equipped with a 40× objective. ZsGreen was excited with a 1030 nm laser. Images were analyzed with Imaris software (Bitplane, Oxford Instruments).

Intra-epidermal DNA "tattoo" vaccination

Mice were anaesthetized, and the thigh was depilated with cream (Veet, Reckitt Benckiser). A 15-μL drop of a 2 mg/mL plasmid DNA solution in endotoxin-free water (B Braun Melsungen AG) was applied to the hairless skin and delivered into the epidermis with a permanent make up tattoo device (MT Derm GmbH), using a sterile disposable 9-needle bar with a needle depth of 1 mm and oscillating frequency of 100 Hz for 45 seconds. For the experiments in which dLNs were analyzed, mice were vaccinated on both thighs.

Cell isolation and flow cytometry

Blood was collected from the tail vein in Microvette CB 300 LH tubes (Sarstedt). Red blood cells were lysed in 0.14 mol/L NH_4Cl, 0.017 mol/L Tris-HCl, pH 7.2 for 1 minute at room temperature. Next, cell samples were centrifuged for 4 minutes at 400 × *g*, resuspended in FACS buffer (PBS with 2% FBS; Antibody Production Services Ltd.) and stained with Alexa Fluor 488–conjugated mAb to CD8 (53-6.7, eBioscience),

PE-Cyanine7–conjugated mAb to CD43 (1B11, BioLegend), PE-conjugated mAb to CD4 (GK1.5, eBioscience), and APC-conjugated H-2K^b/OVA$_{257\text{-}264}$ or H-2D^b/E7$_{49\text{-}57}$ tetramers (produced in house, as described; ref. 24) for 30 minutes at 4°C. To isolate lymphocytes from inguinal dLNs, organs were passed through 100 μmol/L nylon mesh cell strainer (BD), centrifuged for 4 minutes at 400 × *g*, resuspended in FACS buffer, or treated with Liberase TM (Roche), according to the manufacturer's protocol, counted on a NucleoCounter NC-200 (Chemometec) and stained with PE-Cyanine7-conjugated mAb to CD11c (HL3, BD Pharmingen), eFluor 450-conjugated mAb to B220 (RA3-6B2, eBioscience), Alexa Fluor 647–conjugated mAb to I-A/I-E (M5/114.15.2, BioLegend), PerCP/Cy5.5-conjugated mAb to XCR1 (ZET, BioLegend), BUV395-conjugated mAb to CD8α (53-6.7, BD), or mAb to CD11b (M1/70, BD). Live cells were selected based on propidium iodide (PI) or 4′,6-diamidino-2-phenylindole (DAPI) dye exclusion. Flow cytometry was performed using LSR II (BD Biosciences) or Dako Cytomation Cyan cytometers. Data were analyzed using FlowJo software (TreeStar Inc.).

Tumor challenge and adoptive T-cell transfer

Melanoma cell line B16-OVA (25) was injected at 4 × 10^5 cells in 200 μL HBSS s.c. on the flank of recipient mice, 5 days prior to vaccination. Tumors were measured by caliper, and mice were sacrificed when tumors reached the ethical endpoint. OT-I T-cells (5 × 10^4) were adoptively transferred retro-orbitally in 200 μL HBSS into recipient mice, 1 day prior to the first vaccination. Splenic OT-I cells of naïve donor mice were purified to 95% homogeneity using the BD IMag mouse CD8 T lymphocyte enrichment set DM (BD Biosciences).

Antibody treatments

Depleting mAb to CD20 (5D2, Genentech), agonistic mAb to CD27 (RM-3E5; ref. 26), or blocking mAb to CD70 (FR70; ref. 27) were injected i.p. at 100 μg per mouse in 100 μL HBSS directly after DNA vaccination and in case of mAb to CD70 also at days 3, 6, and 9. Antibodies to CD27 and CD70 were kindly made available by Dr. Hideo Yagita (Juntendo University School of Medicine, Tokyo, Japan). Depleting mAb to CD4 (GK1.5, Bio X Cell) was injected i.p. at 200 μg per mouse in 100 μL HBSS twice per week, starting 2 days before DNA vaccination.

In vitro T-cell activation assay

Mice were vaccinated on each side of both thighs, and left and right inguinal dLNs were harvested. Pooled cells were sorted by flow cytometry to isolate ZsGreen$^+$ and ZsGreen$^-$ B220$^+$ cells (B cells) and CD11c$^+$ cells (DCs). Alternatively, they were sorted to obtain XCR1$^+$ and XCR1$^-$ cDC subsets from gated migratory (MHCII^{high}CD11c$^+$) and LN-resident (MHCII^{low}CD11c$^+$) cDC populations (28). OT-I T cells were purified from the spleens of donor mice by cell sorting. They were cocultured with the sorted APCs at in RPMI medium with 10% FBS. After 4 days, T cells were stained with DAPI, or with Alexa Fluor 488–conjugated mAb to CD8 (53-6.7, eBioscience), PE-Cyanine7–conjugated mAb to CD44 (IM7, eBioscience), and LIVE/DEAD Fixable Near-IR Dead Cell Stain Kit (Thermo Fisher Scientific), and analyzed by flow cytometry. In the latter case, cells were also quantified using AccuCount Blank Particles (Spherotech). The number of activated CD8$^+$ T cells was calculated using the formula: (number of added beads × number of acquired live CD8$^+$CD44$^+$ cells)/number of acquired beads.

Statistical analysis

Statistical significance was determined with GraphPad Prism software as indicated in the figure legends.

Results

Delivery of vaccine protein expressed in skin keratinocytes to dLNs

In our "tattoo" vaccination method, keratinocytes are transfected with pDNA encoding the vaccine protein (16). This protein may be delivered to pAPCs in the dLN by passive lymphatic draining from the dermis. Alternatively, or in addition, it may be actively transported from epidermis and/or dermis by locally resident pAPCs (Fig. 1A). Cytosolic versions of the fluorescent proteins dsRed, EGFP, tdTomato, and ZsGreen were tested for their suitability to track vaccine protein delivery to the dLN. Only in case of ZsGreen fluorescent cells were readily detectable in the dLN at 72 hours after vaccination (Fig. 1B). This is in Iine with the relatively high resistance of ZsGreen to intralysosomal degradation and quenching (29). ZsGreen was therefore used in all further experiments.

We followed the fate of the vaccine protein in the skin by intravital multiphoton microscopy of the ear. For this purpose, pDNA was delivered by ballistic transfection to limit damage to the delicate tissue. ZsGreen fluorescence was observed in the epidermis, above the basement membrane at 48 hours after transfection (Fig. 1C), in agreement with keratinocyte transfection (16). We considered that the lipid lammellae that seal keratinocytes together (30) might hamper systemic distribution of the vaccine protein. Lipophilic solvents called penetration enhancers dissolve these lamellae and are used to facilitate drug delivery through the skin (31). The penetration enhancer limonene promoted penetration of cytosolic ZsGreen to the dermis (Fig. 1D). Therefore, throughout our study we used a depilatory cream containing limonene to facilitate antigen delivery to the dermis and dLN. In this setting, after vaccination with cytosolic ZsGreen DCs in the dermis displayed a granular pattern of fluorescence, suggesting that they had endocytosed the vaccine protein (Supplementary Fig. S1A).

Validation of subcellular localizations of ZsGreen protein variants

To monitor T-cell priming efficacy, we used pDNA encoding ZsGreen fused at its C-terminus with an OVA protein fragment encompassing OVA$_{257\text{-}264}$ and OVA$_{323\text{-}339}$ peptides that bind to MHC class I and II, respectively. To examine how localization of ZsGreen-OVA in keratinocytes impacted its delivery to pAPCs and CTL priming, specific localization sequences were fused at its N-terminus. In addition to cytosolic (Cyto) ZsGreen, membrane-associated (PAM), nuclear (NLS), and secretory (SP) ZsGreen-OVA variants were created (Supplementary Fig. S1B). The distinct subcellular localizations of these variants were confirmed by microscopic analysis of *in vitro*–transfected keratinocytes (Fig. 1E). Cyto-ZsGreen-OVA localized in the cytoplasm and was excluded from the ER lumen, as identified by antibody to the chaperone BIP

Published OnlineFirst May 15, 2018; DOI: 10.1158/2326-6066.CIR-17-0408

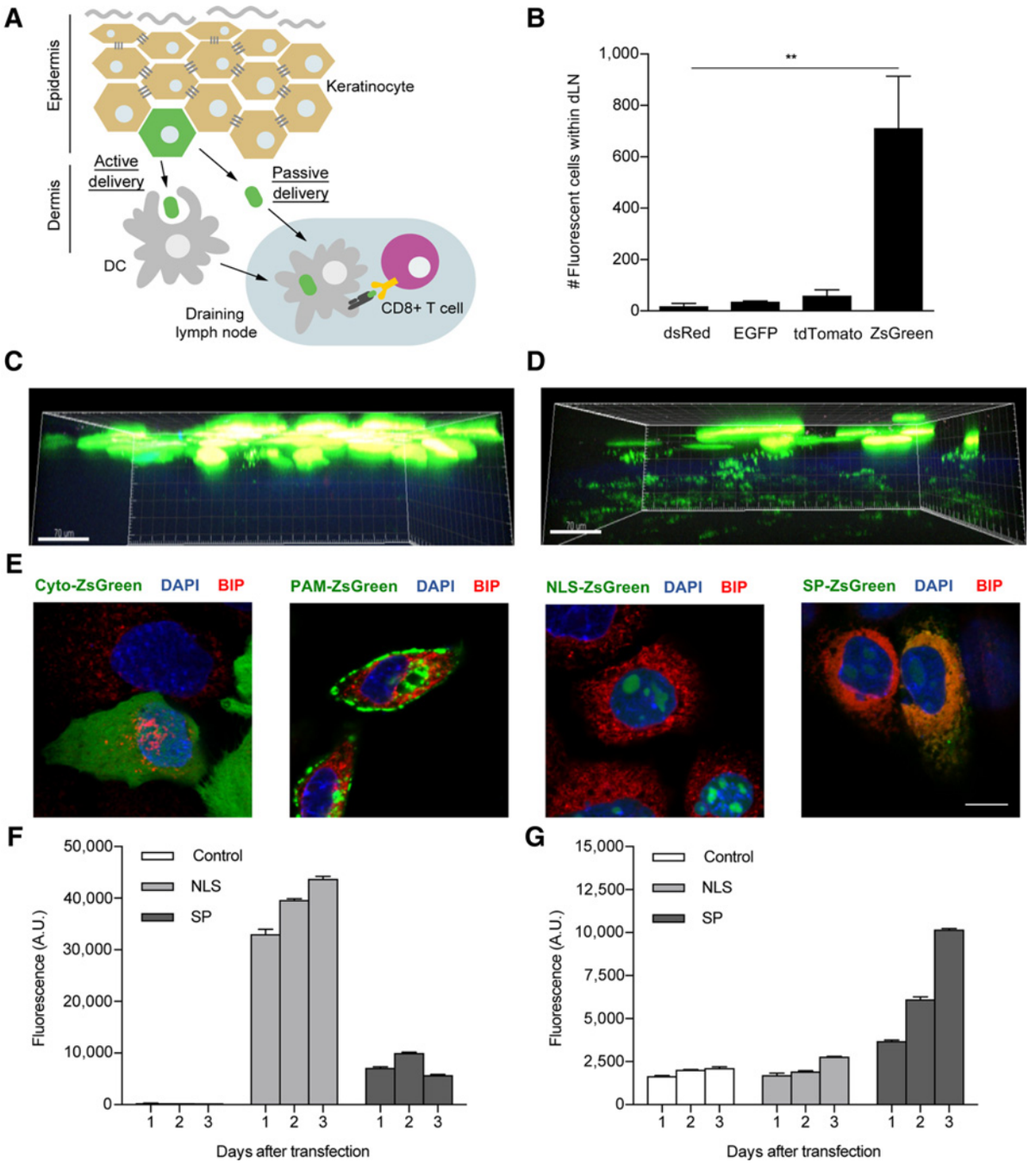

Figure 1.

DNA vaccines encoding modified ZsGreen proteins allow for distinct subcellular localization of antigen in keratinocytes and monitoring of antigen delivery to dLN. **A,** Scheme depicting the cellular scenario of passive or active ZsGreen-OVA antigen delivery from keratinocytes to the dLN. **B,** Mice ($n = 3$ per group) were vaccinated with DNA encoding dsRed, EGFP, tdTomato, or Cyto-ZsGreen. The inguinal dLN was isolated 3 days later and absolute numbers of live fluorescent cells were determined by flow cytometry based on DAPI exclusion. Statistical significance was determined using two-way ANOVA and Tukey posttest (**, $P < 0.01$). **C** and **D,** The pinna of the mouse ear was transfected with DNA encoding Cyto-ZsGreen by gene gun. Fluorescent protein was visualized by live imaging 48 hours later. Transversal skin sections of mice whose skin was not treated (**C**) or treated (**D**) with limonene. The blue autofluorescence denotes the basement membrane that separates epidermis and dermis, based on secondary harmonic generation of collagen (44). **E,** Subcellular localization in *in vitro*–transfected keratinocytes (mTIC) of the four ZsGreen variants relative to the ER lumen (BIP) and the nucleus (DAPI), as examined by CLSM. Scale bar, 10 μm. **F** and **G,** Quantitative analysis of fluorescent signal within HeLa cells (**F**) and their supernatant medium (**G**) at 3 days after transfection with empty vector (Control) or vector encoding NLS- or SP-ZsGreen variants. This experiment with duplicate samples is representative of two. See also Supplementary Fig. S1.

Published OnlineFirst May 15, 2018; DOI: 10.1158/2326-6066.CIR-17-0408

(32). PAM-ZsGreen-OVA localized to the plasma membrane and vesicles, but not in the ER. NLS-ZsGreen-OVA was exclusively present in the nucleus (identified by DAPI staining), whereas SP-ZsGreen-OVA was imported into the ER lumen. Secretion of SP-ZsGreen-OVA, but not NLS-ZsGreen-OVA, was validated by detection of fluorescence in *in vitro*–transfected cells (Fig. 1F) and their supernatant culture medium (Fig. 1G).

Antigen delivery to B cells and DCs in dLNs depends on subcellular localization in keratinocytes

We next examined the impact of vaccine protein localization in keratinocytes on its delivery to pAPCs in the dLN (Supplementary Fig. S2A). Flow cytometric analysis of the dLN postvaccination reproducibly revealed small numbers of live, green fluorescent cells (Supplementary Fig. S2B). For all variants, the number of ZsGreen$^+$ cells in the dLN increased from days 1 to 6 after vaccination (Fig. 2A). Almost all ZsGreen$^+$ cells were MHC class II$^+$, indicating specific delivery to pAPCs (Fig. 2B). After vaccination with Cyto- or PAM-ZsGreen-OVA, more fluorescent pAPCs were recovered from the dLN at all time points of analysis than after vaccination with SP- or NLS-ZsGreen-OVA (Fig. 2A). ZsGreen$^+$ cells included MHCII$^+$/B220$^+$/CD11c$^-$ cells (Fig. 2C; Supplementary Fig. S2C) that were also CD19$^+$ (Supplementary Fig. S2D) and thereby defined as B cells, as well as MHC class II$^+$/B220$^-$ cells that include cDCs and exclude pDCs (Fig. 2D; Supplementary Fig. S2C).

Vaccine proteins were delivered to B cells (Fig. 2C) and DCs (Fig. 2D) in the dLN, with the highest efficiency for Cyto- and PAM-ZsGreen-OVA. Delivery to B cells suggests that at least part of the vaccine protein passively drained to the dLN, because B cells do not carry antigen from the skin. Part of the vaccine protein that localized to DCs may likewise have drained to the dLN, in addition to being actively transported by migratory DCs. Thus, the subcellular localization in keratinocytes impacted the quality and quantity of its delivery to pAPC types in the dLN.

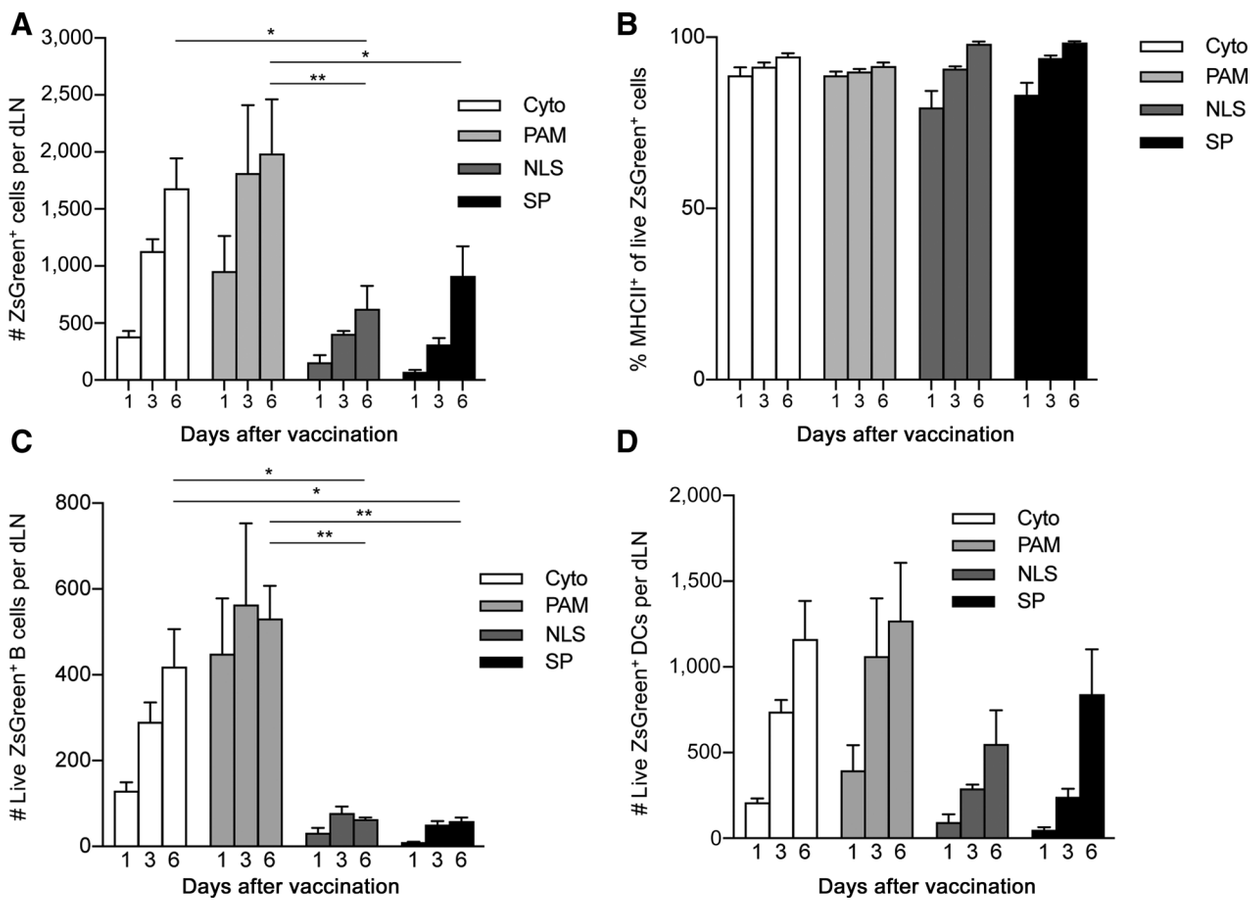

Figure 2.

Impact of subcellular localization of the vaccine protein in keratinocytes on its delivery to pAPCs in the dLN. Mice (n = 3–4 per group) were vaccinated at both flanks with the indicated pDNA constructs encoding ZsGreen-OVA localization variants. Inguinal dLNs were isolated at days 1, 3, or 6 after vaccination and analyzed by flow cytometry. **A,** Number (#) of live ZsGreen$^+$ cells per dLN. **B,** Percentage of MHC class II$^+$ cells among live ZsGreen$^+$ cells in dLN. **C** and **D,** Numbers (#) of live ZsGreen$^+$MHC class II$^+$ B cells (B220$^+$, CD11c$^-$; **C**) or DCs (B220$^-$, CD11c$^+$; **D**) per dLN. Statistical significance was determined using two-way ANOVA and Tukey posttest and is shown for the comparison between the experimental groups at day 6 (*, $P < 0.05$; **, $P < 0.01$). The experiment is representative of two. Error bars, SEM. See also Supplementary Fig. S2.

Published OnlineFirst May 15, 2018; DOI: 10.1158/2326-6066.CIR-17-0408

Secretory ZsGreen-OVA optimally primes CTLs despite suboptimal delivery to dLN

Next, we examined the ability of the four ZsGreen-OVA variants to induce CTL priming. After vaccination, $CD8^+$ T cells recognizing the immunodominant $OVA_{257\text{-}264}$ peptide were monitored longitudinally in peripheral blood by MHC tetramer staining (Fig. 3A; Supplementary Fig. S3A and S3B). At all time points, OVA-specific $CD8^+$ T-cell numbers were highest after vaccination with SP-ZsGreen-OVA (Fig. 3B). This was unexpected, because this variant was less efficiently delivered to pAPCs in the dLN than Cyto- and PAM-ZsGreen-OVA variants.

To assess the quality of $CD8^+$ T-cell priming, we tested whether the CTLs raised could eliminate a tumor. Recipient mice were s.c. implanted with B16-OVA tumor cells, injected with OT-I $CD8^+$ T cells bearing the TCR specific for H-$2K^b$/$OVA_{257\text{-}264}$, and vaccinated with PAM- or SP-ZsGreen-OVA pDNA vaccine (Supplementary Fig. S3C). Vaccination with SP-ZsGreen-OVA raised a $CD8^+$ T-cell response of greater magnitude than vaccination with PAM-ZsGreen-OVA (Fig. 3C). It also resulted in significant tumor control, whereas vaccination with PAM-ZsGreen-OVA did not (Fig. 3D). Thus, despite inefficient delivery to pAPCs, the secretory version of ZsGreen-OVA primed CTLs better than PAM-ZsGreen-OVA.

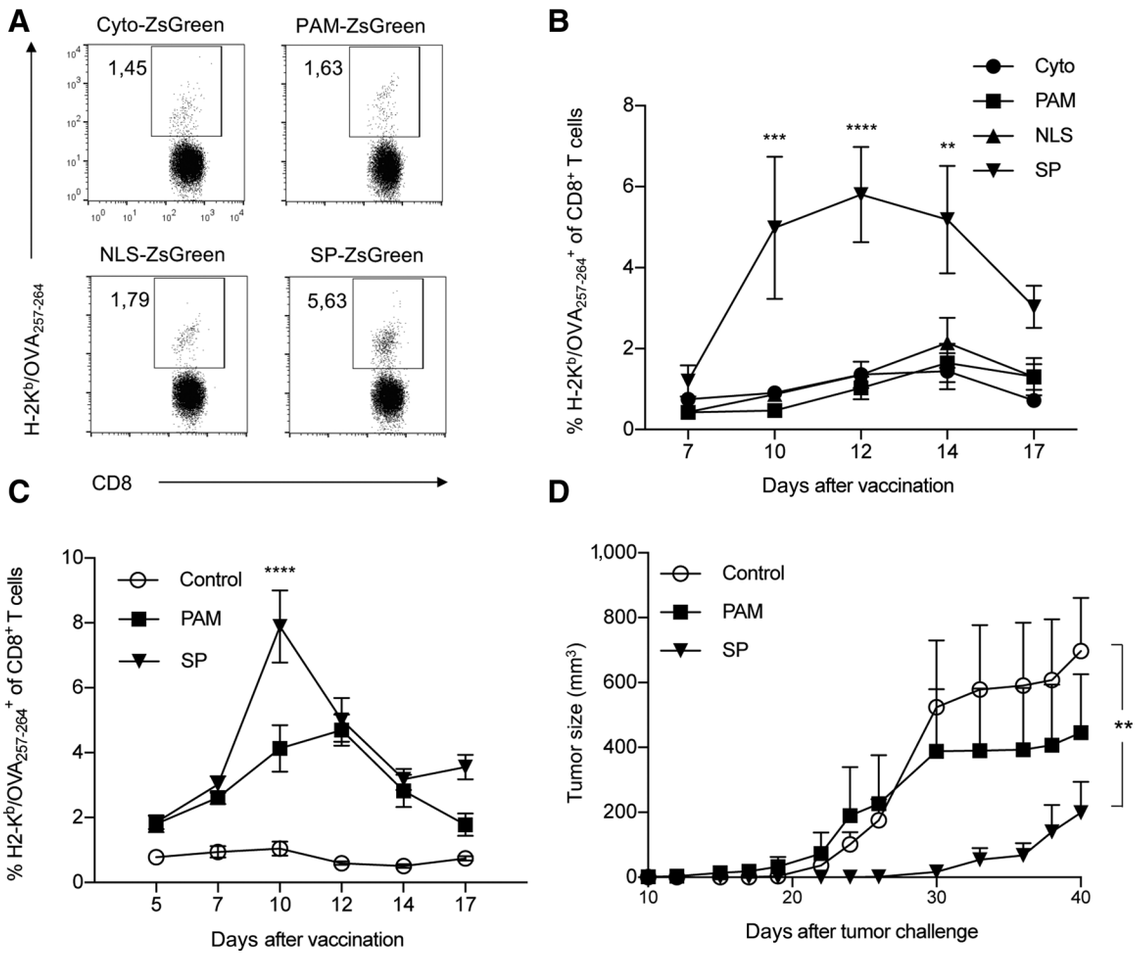

Figure 3.

CTL priming and antitumor activity after vaccination with ZsGreen-OVA variants. **A** and **B,** Mice ($n = 4$–5 per group) received one dose of Cyto-, PAM-, NLS-, or SP-ZsGreen-OVA pDNA vaccine. The vaccine-specific $CD8^+$ T-cell response was followed in time by flow cytometric analysis of blood cells after surface staining with H-$2K^b$/$OVA_{257\text{-}264}$ tetramers and mAb to CD8. The experiment is representative of three. **A,** Representative staining of blood cells at day 12 after vaccination. Numbers in plots indicate the percentage of H-$2K^b$/$OVA_{257\text{-}264}{}^+$ cells within the $CD8^+$ T-cell population (box). **B,** The percentage of H-$2K^b$/$OVA_{257\text{-}264}{}^+$ cells within the $CD8^+$ T-cell population in blood at the indicated days after vaccination with the ZsGreen-OVA variants. Statistical significance was determined using two-way ANOVA and Tukey posttest (**, $P < 0.01$; ***, $P < 0.001$; ****, $P < 0.0001$). **C** and **D,** Mice ($n = 8$ per group) were implanted s.c. with B16-OVA tumor cells at day −5 and adoptively transferred with OT-I T-cells at day −1. They were vaccinated with pDNA encoding PAM- or SP-ZsGreen-OVA at days 0, 3, and 6. Control mice were vaccinated with water without DNA. **C,** The percentage of H-$2K^b$/$OVA_{257\text{-}264}{}^+$ cells within the $CD8^+$ T-cell population in blood at the indicated days after vaccination. Data from PAM- and SP-ZsGreen-OVA groups were statistically compared using two-tailed Student *t* test (****, $P < 0.0001$). **D,** Mean tumor sizes as measured by caliper at the indicated time points after tumor challenge. The experiment is representative of two. Statistical comparison was determined for day 40 after tumor challenge using two-tailed Student *t* test (**, $P < 0.01$). See also Supplementary Fig. S3.

Published OnlineFirst May 15, 2018; DOI: 10.1158/2326-6066.CIR-17-0408

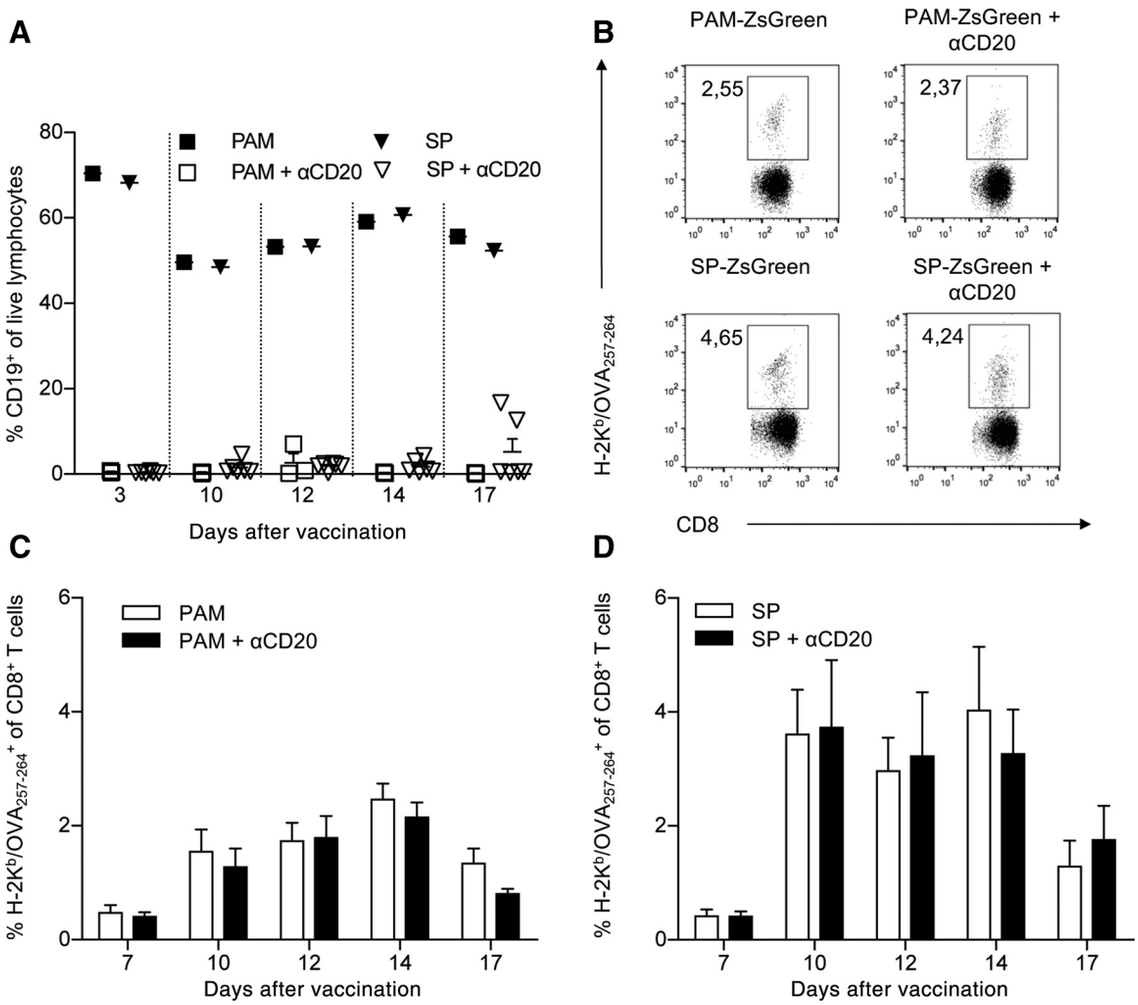

Figure 4.

Assessing the relevance of B cells for CD8$^+$ T-cell priming after intra-epidermal DNA vaccination. Mice (n = 4–6 per group) received one dose of PAM- or SP-ZsGreen-OVA pDNA vaccine and were injected i.p. with B-cell–depleting mAb to CD20 or not. **A,** Presence of B-cells (CD19$^+$) in the blood of individual mice in the respective experimental groups at the indicated days after vaccination. **B,** Representative flow cytometric analysis of blood cells at day 14 after vaccination. Numbers indicate the percentage of H-2K^b/OVA$_{257\text{-}264}^+$ cells within the CD8$^+$ T-cell population. **C** and **D,** The magnitude of the antigen-specific CD8$^+$ T-cell response as followed by flow cytometric analysis of blood cells after surface staining with H-2K^b/OVA$_{257\text{-}264}$ tetramers and mAb to CD8. The experiment is representative of two. Statistical significance was determined using a two-tailed Student t test (n.s., $P > 0.05$). See also Supplementary Fig. S4.

This result suggests that the nature of the pAPCs receiving the antigenic protein was decisive for CTL priming.

B cells are irrelevant for CD8$^+$ T-cell priming after intra-epidermal DNA vaccination

To examine the role of B cells as pAPCs for CD8$^+$ T-cell priming, mice were treated with a B cell–depleting mAb to CD20 (Supplementary Fig. S4). B-cell depletion was effective, as judged by the absence of B cells in blood throughout the entire kinetics of the CD8$^+$ T-cell response (Fig. 4A). B-cell depletion did not affect CD8$^+$ T cell responses after vaccination with PAM- (Fig. 4B and C) or SP-ZsGreen-OVA (Fig. 4B and D). Thus, B cells, even though they take up antigen in the dLN, were not involved in CD8$^+$ T-cell priming in this therapeutic vaccination strategy.

Deficient activation status of DCs limits CD8$^+$ T-cell priming

We next investigated the CD8$^+$ T-cell priming capacity of ZsGreen$^+$ APCs from the dLN in an *in vitro* assay (Fig. 5A). We vaccinated with PAM-ZsGreen-OVA, because in that setting we could recover sufficient ZsGreen$^+$ cells from the dLN for *in vitro* testing. ZsGreen$^-$ B cells and DCs were also tested. As a negative control, we vaccinated with a construct encoding mutated OVA$_{257\text{-}264}$ peptide lacking MHC anchor residues (PAM-ZsGreen-OVA^{MUT}). The pAPCs were cocultured with OT-I OVA–specific CD8$^+$ T cells, with or without CpG as a mimic of pathogen stimulation, or agonistic mAb to CD40 as a mimic of CD4$^+$ T-cell help (8). After 4 days, activated OT-I T cells were enumerated (Supplementary Fig. S5A).

ZsGreen$^+$ DCs from mice vaccinated with PAM-ZsGreen-OVA^{WT} could not activate OT-I T cells, unless they were activated

Published OnlineFirst May 15, 2018; DOI: 10.1158/2326-6066.CIR-17-0408

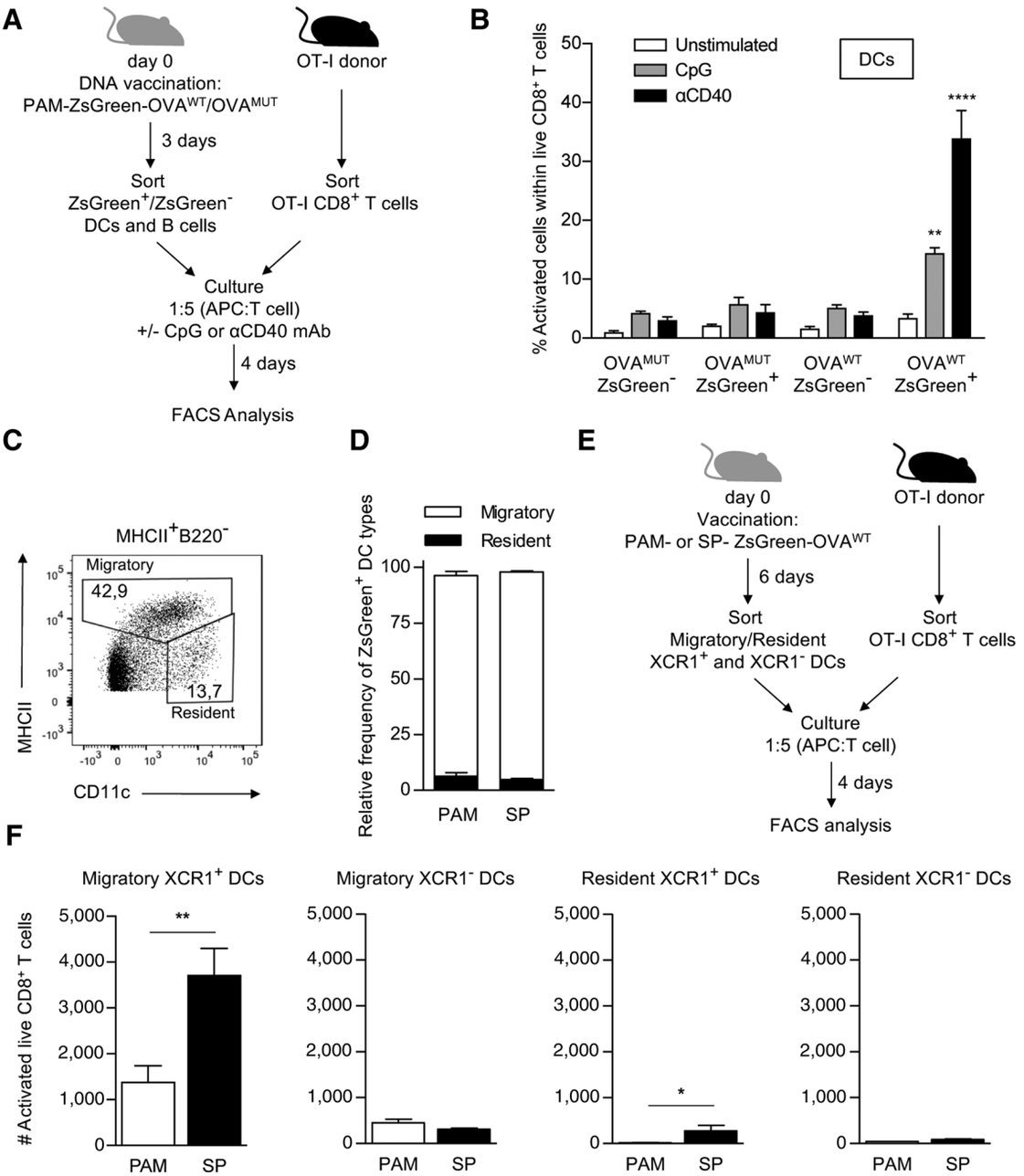

Figure 5.

Nature and CD8$^+$ T-cell priming ability of antigen-loaded DCs from dLNs. **A** and **B,** Mice ($n = 7$ per group) received one dose of pDNA vaccine encoding PAM-ZsGreen-OVA^{WT} or nonpresentable PAM-ZsGreen-OVA^{MUT}. At day 3 after vaccination, ZsGreen positive (+) and negative (–) DCs or B cells were flow cytometrically sorted from the dLN and divided in triplicate samples. Next, they were cocultured with naïve OT-I CD8$^+$ T cells (pooled from 2 mice) with or without CpG or mAb to CD40. **A,** Schematic overview of experimental procedure. **B,** Percentage of live (DAPI$^-$), activated OT-I CD8$^+$ T cells diagnosed by blast formation (Supplementary Fig. S5A) after coculture with ZsGreen positive (+) or negative (–) DCs. Statistical significance was determined using two-way ANOVA and Tukey posttest and is indicated for comparison between unstimulated groups and groups stimulated with CpG or mAb to CD40 (**, $P < 0.01$; ****, $P < 0.0001$). The experiment is representative of two. **C** and **D,** Mice ($n = 3$ per group) received PAM- or SP-ZsGreen-OVA pDNA vaccine at both flanks. At day 6 after vaccination, inguinal dLNs were analyzed by flow cytometry. **C,** Representative flow cytometric analysis of gated MHCII$^+$B220$^-$ cells to diagnose migratory and resident DCs based on MHCII and CD11c expression (28). **D,** Relative distribution of ZsGreen$^+$ DCs over migratory and resident populations. The experiment is representative of three. **E** and **F,** Mice ($n = 4$ per group) were vaccinated with pDNA encoding PAM- or SP-ZsGreen-OVA^{WT}. Migratory or resident XCR1$^+$ and XCR1$^-$ cells were flow cytometrically sorted from the dLN, divided over triplicate samples and cocultured with naïve OT-I CD8$^+$ T cells with or without CpG or mAb to CD40. **E,** Schematic overview of experimental procedure. **F,** Number (#) of live, activated OT-I CD8$^+$ T cells diagnosed by expression of CD44 after coculture with unstimulated DCs. The experiment is representative of three. Statistical significance was determined using two-tailed Student *t* test (*, $P < 0.05$; **, $P < 0.01$). See also Supplementary Fig. S5.

in vitro (Fig. 5B; Supplementary Fig. S5A). B cells did not prime $CD8^+$ T cells, even after *in vitro* activation (Supplementary Fig. S5B), in agreement with our finding that B cells did not contribute to $CD8^+$ T-cell priming *in vivo*. These data suggested that a deficient activation status of antigen-loaded DCs in dLN limited $CD8^+$ T-cell priming after vaccination with PAM-ZsGreen-OVA.

Secretory protein is superior in engaging $XCR1^+$ cDCs that have $CD8^+$ T-cell priming ability

We next examined to which specific DC subset(s) the vaccine antigen was delivered. After vaccination with PAM- or SP-ZsGreen-OVA, MHC class II^{high} migratory and MHC class II^{low} LN-resident DC populations could easily be discerned in the dLN (Fig. 5C). As described (28), the MHC class II^{low} population was enriched for LN-resident $XCR1^+CD8^+$ cDCs (5, 33), and the MHC class II^{high} population did not contain cells of this phenotype (Supplementary Fig. S5C). PAM- and SP-ZsGreen-OVA proteins mainly localized to migratory cDCs and to a lesser extent to LN-resident cDCs (Fig. 5D; Supplementary Fig. S5D). Among both migratory and LN-resident cDCs, PAM-ZsGreen was primarily found in the $CD11b^+$ subset and to a lesser extent in the $XCR1^+$ subset (Supplementary Fig. S5E). The distribution of SP-ZsGreen-OVA over these two DC subsets could not be reliably assessed within migratory and LN-resident populations. We conclude that PAM-ZsGreen-OVA localizes to migratory cDCs and—to a lesser extent—to LN-resident cDCs in the dLN, but that these cDCs have no $CD8^+$ T-cell priming potential, due to a deficient activation status.

To understand why SP-ZsGreen-OVA was superior in CTL induction, we compared the *ex vivo* priming ability of migratory and LN-resident DC subsets carrying PAM- or SP-ZsGreen-OVA. For this purpose, we sorted these subsets irrespective of ZsGreen fluorescence on day 6, when the frequency of $ZsGreen^+$ DCs was similar in both settings (Fig. 2D). In this way, we obtained enough DCs for the experiments and included DCs that might have digested the ZsGreen-OVA into smaller presentable peptides (Fig. 5E). The migratory $XCR1^+$ cDC subset presenting SP-ZsGreen-OVA had clearly detectable OT-I priming ability *ex vivo* (Fig. 5F; Supplementary Fig. S5F), whereas the priming ability of the migratory $XCR1^+$ cDC subset presenting PAM-ZsGreen-OVA was significantly lower (Fig. 5F). The migratory $XCR1^-$ cDC subsets isolated from either vaccination setting could not prime OT-I T cells. Among LN-resident cDC subsets, only the $XCR1^+$ subset from the SP-ZsGreen-OVA setting revealed *ex vivo* priming ability (Fig. 5F). We conclude that SP-ZsGreen-OVA is superior over PAM-ZsGreen-OVA in engaging the $XCR1^+$ cDCs subsets that present the vaccine antigen. Together, the data suggest that the activation status of $XCR1^+$ DCs, rather than their antigen loading, explained the differential ability of SP- and PAM-ZsGreen-OVA to induce $CD8^+$ T-cell priming.

$CD8^+$ T-cell priming after intra-epidermal DNA vaccination is completely reliant on $CD4^+$ T-cell help

$CD4^+$ T cells can activate DCs via CD40 signaling, which promotes CTL priming, especially when pathogen-derived or "danger" signals are limiting (8, 9). We therefore examined the involvement of $CD4^+$ T-cell help to $CD8^+$ T-cell priming after vaccination with PAM- and SP-ZsGreen-OVA. A "help-deficient" setting was created by efficient antibody-based $CD4^+$ T-cell depletion (Fig. 6A; Supplementary Fig. S6A). $CD4^+$ T-cell depletion abrogated $CD8^+$ T-cell responses to both PAM- (Fig. 6B and C) and SP-ZsGreen-OVA (Fig. 6B and D), indicating that $CD8^+$ T-cell priming in response to both ZsGreen-OVA versions fully depended on $CD4^+$ T-cell help.

The MHC class II epitope in the vaccine evoked a $CD4^+$ T-cell response to both ZsGreen-OVA versions, as assessed by the presence of $CD4^+$ T cells with an effector phenotype (Supplementary Fig. S6). The magnitude of the $CD4^+$ T-cell response did not differ between both vaccination settings. However, delivery of $CD4^+$ T-cell help for the CTLs response at a specific time and place in the dLN is dependent on chemokine-guided T cell and DC migration (11), which may well be distinct in both settings. To assess to which extent $CD4^+$ T-cell help to the CTL response was delivered, we next performed experiments in which "help" was supplemented by a CD27 agonist antibody.

CD27 costimulation reveals that SP-ZsGreen-OVA maximally solicits $CD4^+$ T-cell help

$CD4^+$ T-cell help is delivered to $CD8^+$ T cells via the CD27 costimulatory receptor, upon engagement by its ligand CD70 that is expressed on CD40-activated DCs (refs. 9, 34–36; Fig. 7A). To test the involvement of CD27/CD70 costimulation in the $CD8^+$ T-cell response to PAM- or SP-ZsGreen-OVA, mice were treated with a mAb that blocks CD70 (Fig. 7A; Supplementary Fig. S7A). CD70 blocking significantly reduced the magnitude of the $CD8^+$ T-cell response to SP-ZsGreen-OVA, but not to PAM-ZsGreen-OVA (Fig. 7B), suggesting deficient "help" in the latter setting. Deliberate engagement of CD27 with an agonistic antibody can mimic $CD4^+$ T-cell help (35, 36). We treated mice with CD27 agonist mAb to examine whether deficient "help" limited $CD8^+$ T-cell priming after vaccination with any of the ZsGreen-OVA variants (Fig. 7A; Supplementary Fig. S7B). Treatment with CD27 agonist mAb significantly increased the $CD8^+$ T-cell response to PAM- (Fig. 7C), Cyto- (Fig. 7E), and NLS-ZsGreen-OVA (Fig. 7F), but not to SP-ZsGreen-OVA (Fig. 7D). This result indicates that the secretory SP-ZsGreen-OVA protein maximally solicits $CD4^+$ T-cell help, whereas the other localization variants do not. This capacity explains its superiority among the ZsGreen-OVA localization variants in raising a CTL response.

Discussion

Vaccine protein that was expressed in keratinocytes after DNA tattooing of depilated skin reached pAPCs in the underlying dermis. We could track vaccine protein to B cells and specific DC subsets in the dLN by virtue of fluorescence and *in vitro* $CD8^+$ T-cell priming assays. Vaccine protein can reach B cells by lymphatic draining from the dermis to the subcapsular sinus of the dLN. There, it can pass the fenestrated sinus floor and reach the underlying B-cell follicle (37), where B cells can endocytose the antigen. B cells have been reported to cross-present antigen in MHC class I (38), albeit less efficiently than cDCs. In our setting, however, antigen-loaded B cells could not prime $CD8^+$ T cells, even after activation *in vitro*, and B cells were irrelevant for *in vivo* $CD8^+$ T-cell priming. Other investigators did find a contribution of B cells to $CD8^+$ T-cell priming in a comparable vaccination setting (39). It is not clear how this is accomplished, because naïve B cells are physically separated from naïve T cells in the LN. Upon their activation,

Published OnlineFirst May 15, 2018; DOI: 10.1158/2326-6066.CIR-17-0408

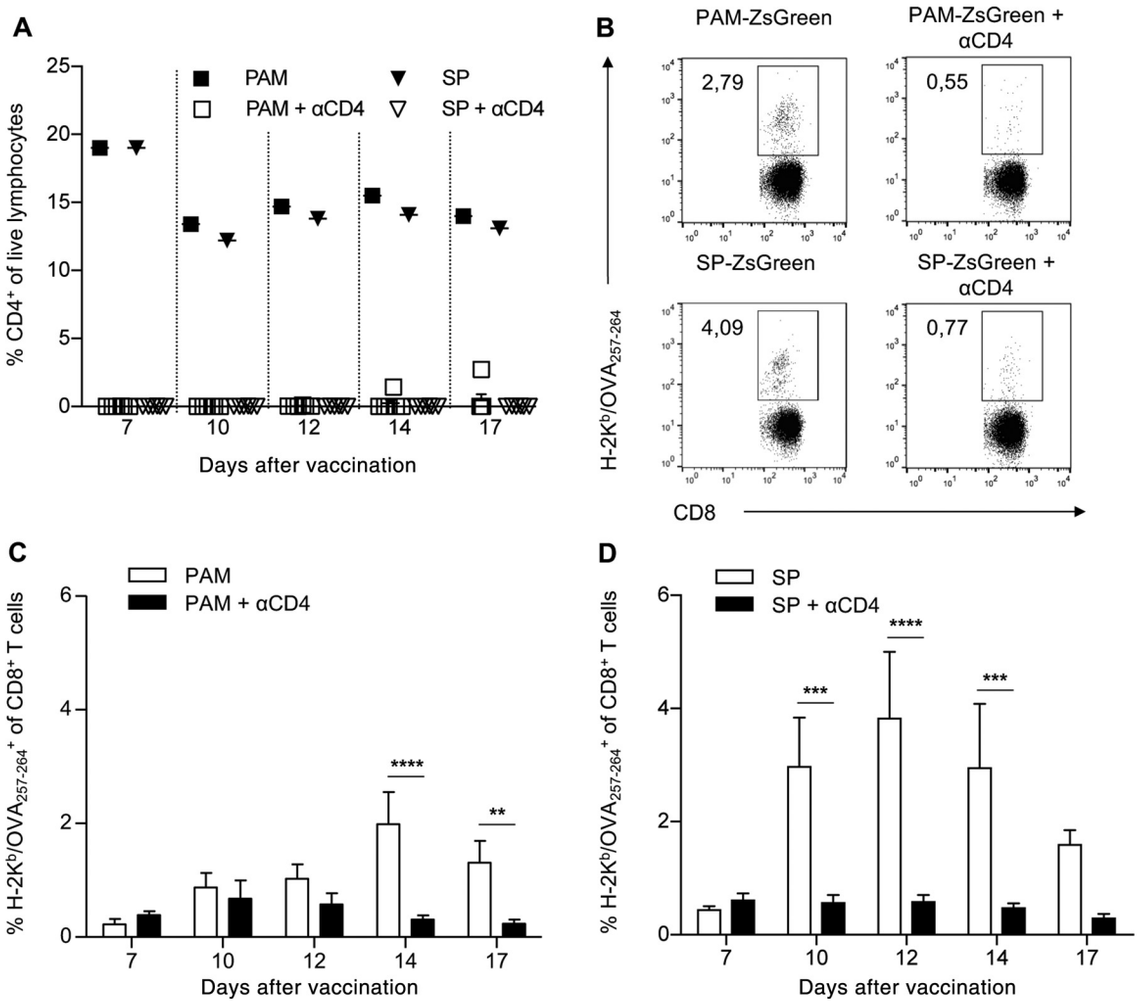

Figure 6.

$CD4^+$ T-cell help is required to raise a $CD8^+$ T-cell response upon intra-epidermal DNA vaccination. Mice received one dose of pDNA vaccine encoding PAM- or SP-ZsGreen-OVA. To deplete $CD4^+$ T cells, mice were injected i.p. with mAb to CD4 twice per week, starting 2 days before vaccination. The antigen-specific $CD8^+$ T-cell response was followed in time by flow cytometric analysis of blood cells after surface staining with H-$2K^b/OVA_{257-264}$ tetramers and mAb to CD8. **A,** The percentage of $CD4^+$ T cells within live lymphocytes determined in blood of mice that had received mAb to CD4 or not. **B,** Representative staining of blood cells of mice that had received mAb to CD4 or not at day 14 after vaccination with PAM- or SP-ZsGreen-OVA. Numbers indicate the percentage of H-$2K^b/OVA_{257-264}{}^+$ cells within the $CD8^+$ T-cell population. **C** and **D,** The percentage of H-$2K^b/OVA_{257-264}{}^+$ cells within the $CD8^+$ T-cell population in blood of mice that had received mAb to CD4 or not after vaccination with PAM- (**C**) or SP-ZsGreen-OVA (**D**). The experiment is representative of two ($n = 4$–6). Statistical significance was determined using two-tailed Student t test (**, $P < 0.01$; ***, $P < 0.001$; ****, $P < 0.0001$). See also Supplementary Fig. S6.

B cells move to the border of the B-cell follicle where they meet helper $CD4^+$ helper T cells. Activated B cells can also meet activated $CXCR5^+$ $CD8^+$ T cells at this site (40), but these T cells do not become CTLs. Possibly, B cells can indirectly contribute to CTL priming, e.g., by antigen capture and transfer to other pAPCs.

Migratory cDCs were more efficiently loaded with vaccine protein than LN-resident cDCs in our setting. We did not find $ZsGreen^+$ Langerhans' cells in the dLN, based on CD207 (Langerin) phenotyping. In agreement with this, intravital imaging revealed that most MHC class II^+ cells that reside in the epidermis (i.e., Langerhans cells) leave the injection site within 30 minutes after a pDNA tattoo, when antigen expression is minimal. We also did not find $ZsGreen^+$ macrophages in the dLN, based on F4/80 staining (results not shown). Thus, $CD8^+$ T-cell priming in our setting relied on cDCs, rather than on other pAPC types. The migratory cDCs loaded with PAM-ZsGreen-OVA *in vivo* could not prime $CD8^+$ T cells unless they were activated *in vitro*. Nonactivated, migratory cDCs bring self-antigens from peripheral tissues to dLNs at steady state and thus promote T-cell tolerance (41). PAM-ZsGreen-OVA was found more in $CD11b^+$ than in $XCR1^+$ migratory cDCs, but the $XCR1^+$ subset was better able to prime $CD8^+$ T cells after activation *in vitro*. This is in line with the superior cross-presentation ability of this cDC lineage (42) and argues for uptake of antigen by endocytosis in the dermis. Thus, after

Published OnlineFirst May 15, 2018; DOI: 10.1158/2326-6066.CIR-17-0408

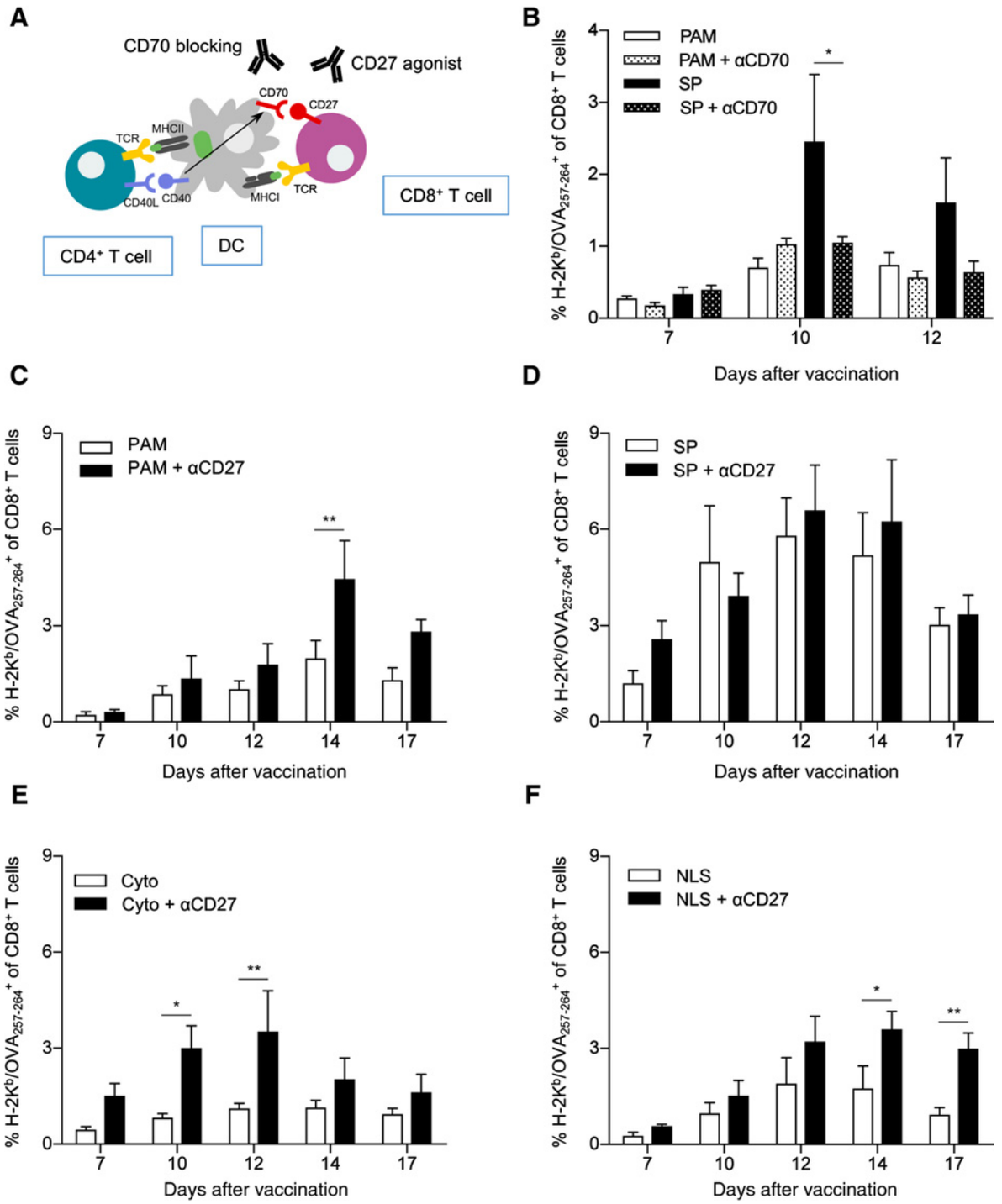

Figure 7.

SP-ZsGreen-OVA maximally solicits CD27/CD70 costimulation. **A,** Scheme depicting the role of CD27/CD70 costimulation in delivery of $CD4^+$ T-cell help for the CTL response. **B–F,** Mice ($n = 4$–6) received one dose of Cyto-, PAM-, NLS-, or SP-ZsGreen-OVA pDNA vaccine and were injected i.p. with blocking mAb to CD70 (**B**) or agonistic mAb to CD27 (**C–F**). The antigen-specific $CD8^+$ T-cell response was followed in time by flow cytometric analysis of blood cells after surface staining with H-$2K^b$/$OVA_{257\text{-}264}$ tetramers and mAb to CD8. **B,** The percentage of H-$2K^b$/$OVA_{257\text{-}264}{}^+$ cells within the $CD8^+$ T-cell population in blood of mice that had received mAb to CD70 or not after vaccination with PAM- or SP-ZsGreen-OVA. Statistical significance was determined using two-way ANOVA and Tukey posttest (*, $P < 0.05$). **C–F,** The percentage of H-$2K^b$/$OVA_{257\text{-}264}{}^+$ cells within the $CD8^+$ T-cell population in blood of mice that had received mAb to CD27 mAb or not after vaccination with Cyto- (**C**), PAM- (**D**), NLS- (**E**), or SP-ZsGreen-OVA (**F**). The experiment is representative of two (**B**) or three (**C–F**). Statistical significance was determined using two-tailed Student *t* test (*, $P < 0.05$; **, $P < 0.01$). See also Supplementary Fig. S7.

Published OnlineFirst May 15, 2018; DOI: 10.1158/2326-6066.CIR-17-0408

PAM-ZsGreen-OVA expression in keratinocytes, migratory cDCs took up the vaccine protein, but did not receive the appropriate activation stimuli to become capable of priming $CD8^+$ T-cells.

Vaccination with SP-ZsGreen-OVA led to the best CTL priming, even though PAM-Zs-Green-OVA was more efficiently loaded into cDCs. The relative distribution of both vaccine proteins over migratory and LN-resident cDCs was comparable. Migratory $XCR1^+$ cDCs were much better at priming a $CD8^+$ T-cell response *in vitro* when taken from mice vaccinated with SP-ZsGreen-OVA, as compared with PAM-ZsGreen-OVA. The activation status, rather than antigen-loading and presentation, limited the ability of PAM-ZsGreen-OVA cDCs to prime OT-I T cells. The data suggest that SP-ZsGreen-OVA better activates $XCR1^+$ migratory cDCs *in vivo* than does PAM-ZsGreen-OVA. At present, we do not know why this is the case. Different modes of vaccine protein release from keratinocytes and different modes of vaccine protein uptake by migratory $XCR1^+$ cDCs may translate into differential engagement and/or activation of these DCs. Alternatively, the ER localization of SP-ZsGreen-OVA protein may underlie optimal CTL responsiveness as previously suggested (18). Possibly, ER localization of the vaccine protein results in optimal release of danger signals from keratinocytes and thereby lead to optimal activation of migratory $XCR1^+$ cDCs in the dermis. SP-ZsGreen-OVA was also superior in invoking $CD4^+$ T-cell help, which may be linked to its ability to activate migratory cDCs.

We conclude that in pDNA vaccination, just including helper epitopes in the vaccine protein is not sufficient to secure $CD4^+$ T-cell help. The subcellular location of the antigen in the transfected cells impacts on the delivery of pAPC subtypes in a quantitative and qualitative manner. It will be useful to have a diagnostic tool in human to assess whether help has been delivered after vaccination. Our data suggest that activation of migratory $XCR1^+$ cDCs may be important to ensure delivery of help. In our DNA vaccination model, targeting vaccine protein to the secretory route of keratinocytes was optimal as compared with a cytosolic, plasma membrane/endosomal, or nuclear localization to engage migratory $XCR1^+$ cDCs, solicit $CD4^+$ T-cell help, and prime a CTL response. "Helpless" $CD8^+$ T-cell priming could largely be rescued by systemic administration of CD27 agonist antibody. Other vaccination platforms, such as long peptide- (1) and RNA- (43) based vaccination may likewise be supported, in case delivery of help may prove suboptimal. Together, these insights may help to rationally optimize therapeutic DNA vaccination strategies.

Disclosure of Potential Conflicts of Interest

M.F. Krummel is director of Piony Immunotherapeutics. J. Borst reports receiving a commercial research grant from Aduro Biotech Europe. No potential conflicts of interest were disclosed by the other authors.

Authors' Contributions

Conception and design: N. Bąbała, J. Borst, A.D. Bins
Development of methodology: N. Bąbała, E. de Vries, A.D. Bins
Acquisition of data (provided animals, acquired and managed patients, provided facilities, etc.): N. Bąbała, A. Bovens, E. de Vries, V. Iglesias-Guimarais, T. Ahrends, M. Krummel, J. Borst
Analysis and interpretation of data (e.g., statistical analysis, biostatistics, computational analysis): N. Bąbała, A. Bovens, T. Ahrends, J. Borst, A.D. Bins
Writing, review, and/or revision of the manuscript: N. Bąbała, M.F. Krummel, J. Borst, A.D. Bins
Administrative, technical, or material support (i.e., reporting or organizing data, constructing databases): N. Bąbała, A.D. Bins
Study supervision: J. Borst, A.D. Bins

Acknowledgments

This work was supported by grant NKI 2012-5397 of the Dutch Cancer Society and by grant 91610005 of ZonMW.

We thank Drs. A. Sonnenberg, H. Yagita, and R. Arens, as well as Genentech for kindly providing reagents, Drs. J. den Haan and W. Kastenmüller for helpful discussions, M. van Baalen for technical advice, Drs. I. Verbrugge and Y. Xiao for critical reading of the manuscript and advice, and the Flow Cytometry, Animal Pathology and Experimental Animal facilities of the Netherlands Cancer Institute for technical assistance.

The costs of publication of this article were defrayed in part by the payment of page charges. This article must therefore be hereby marked *advertisement* in accordance with 18 U.S.C. Section 1734 solely to indicate this fact.

Received August 1, 2017; revised February 28, 2018; accepted May 9, 2018; published first May 15, 2018.

References

1. Melief CJM, van Hall T, Arens R, Ossendorp F, van der Burg SH. Therapeutic cancer vaccines. J Clin Invest 2015;125:3401–12.
2. Steinman RM. Dendritic cells in vivo: a key target for a new vaccine science. Immunity 2008;29:319–24.
3. Bernhard CA, Ried C, Kochanek S, Brocker T. CD169+ macrophages are sufficient for priming of CTLs with specificities left out by cross-priming dendritic cells. Proc Natl Acad Sci USA 2015;112:5461–6.
4. Colluru VT, McNeel DG. B lymphocytes as direct antigen-presenting cells for anti-tumor DNA vaccines. Oncotarget 2016;7:67901–18.
5. Murphy TL, Grajales-Reyes GE, Wu X, Tussiwand R, Briseno CG, Iwata A, et al. Transcriptional control of dendritic cell development. Annu Rev Immunol 2016;34:93–119.
6. Iwasaki A, Medzhitov R. Control of adaptive immunity by the innate immune system. Nat Immunol 2015;16:343–53.
7. Wu J, Chen ZJ. Innate immune sensing and signaling of cytosolic nucleic acids. Annu Rev Immunol 2014;32:461–88.
8. Castellino F, Germain RN. Cooperation between CD4+ and CD8+ T cells: when, where, and how. Annu Rev Immunol 2006;24:519–540.
9. Bedoui S, Heath WR, Mueller SN. CD4(+) T-cell help amplifies innate signals for primary CD8(+) T-cell immunity. Immunol Rev 2016;272:52–64.
10. Ott PA, Hu Z, Keskin DB, Shukla SA, Sun J, Bozym DJ, et al. An immunogenic personal neoantigen vaccine for patients with melanoma. Nature 2017;547:217–21.
11. Eickhoff S, Brewitz A, Gerner MY, Klauschen F, Komander K, Hemmi H, et al. Robust anti-viral immunity requires multiple distinct T cell-dendritic cell interactions. Cell 2015;162:1322–37.
12. Hor JL, Whitney PG, Zaid A, Brooks AG, Heath WR, Mueller SN. Spatiotemporally distinct interactions with dendritic cell subsets facilitates CD4+ and CD8+ T cell activation to localized viral infection. Immunity 2015;43:554–65.
13. Kitano M, Yamazaki C, Takumi A, Ikeno T, Hemmi H, Takahashi N, et al. Imaging of the cross-presenting dendritic cell subsets in the skin-draining lymph node. Proc Natl Acad Sci USA 2016;113:1044–9.
14. Romani N, Thurnher M, Idoyaga J, Steinman RM, Flacher V. Targeting of antigens to skin dendritic cells: possibilities to enhance vaccine efficacy. Immunol Cell Biol 2010;88:424–30.
15. Bins AD, Jorritsma A, Wolkers MC, Hung C-F, Wu T-C, Schumacher TNM, et al. A rapid and potent DNA vaccination strategy defined by in vivo monitoring of antigen expression. Nat Med 2005;11:899–904.

16. Bins AD, van Rheenen J, Jalink K, Halstead JR, Divecha N, Spencer DM, et al. Intravital imaging of fluorescent markers and FRET probes by DNA tattooing. BMC Biotechnol 2007;7:2.
17. Verstrepen BE, Bins AD, Rollier CS, Mooij P, Koopman G, Sheppard NC, et al. Improved HIV-1 specific T-cell responses by short-interval DNA tattooing as compared to intramuscular immunization in non-human primates. Vaccine 2008;26:3346–51.
18. Oosterhuis K, Aleyd E, Vrijland K, Schumacher TN, Haanen JB. Rational design of DNA vaccines for the induction of human papillomavirus type 16 E6- and E7-specific cytotoxic T-cell responses. Hum Gene Ther 2012; 23:1301–12.
19. Matz MV, Fradkov AF, Labas YA, Savitsky AP, Zaraisky AG, Markelov ML, et al. Fluorescent proteins from nonbioluminescent Anthozoa species. Nat Biotechnol 1999;17:969–73.
20. Navarro-Lérida I, Álvarez-Barrientos A, Gavilanes F, Rodriguez-Crespo I. Distance-dependent cellular palmitoylation of de-novo-designed sequences and their translocation to plasma membrane subdomains. J Cell Sci 2002;115:3119–30.
21. Raymond K, Kreft M, Song J-Y, Janssen H, Sonnenberg A. Dual role of α6β4 integrin in epidermal tumor growth: tumor-suppressive versus tumor-promoting function. Mol Biol Cell 2007;18:4210–21.
22. Sivamani E, DeLong RK, Qu R. Protamine-mediated DNA coating remarkably improves bombardment transformation efficiency in plant cells. Plant Cell Rep 2009;28:213–21.
23. Bullen A, Friedman RS, Krummel MF. Two-photon imaging of the immune system: a custom technology platform for high-speed, multicolor tissue imaging of immune responses. Curr Top Microbiol Immunol 2009;334: 1–29.
24. Altman JD, Moss PA, Goulder PJ, Barouch DH, McHeyzer-Williams MG, Bell JI, et al. Phenotypic analysis of antigen-specific T lymphocytes. Science 1996;274:94–6.
25. Keller AM, Schildknecht A, Xiao Y, van den Broek M, Borst J. Expression of costimulatory ligand CD70 on steady-state dendritic cells breaks CD8+ T cell tolerance and permits effective immunity. Immunity 2008;29:934–46.
26. Sakanishi T, Yagita H. Anti-tumor effects of depleting and non-depleting anti-CD27 monoclonal antibodies in immune-competent mice. Biochem Biophys Res Commun 2010;393:829–35.
27. Oshima H. Characterization of murine CD70 by molecular cloning and mAb. Int Immunol 1998;10:517–26.
28. Gerner M, Kastenmuller W, Ifrim I, Kabat J, Germain R. Histo-cytometry: a method for highly multiplex quantitative tissue imaging analysis applied to dendritic cell subset microanatomy in lymph nodes. Immunity 2012;37:364–76.
29. Stepanenko OV, Verkhusha VV, Kazakov VI, Shavlovsky MM, Kuznetsova IM, Uversky VN, et al. Comparative studies on the structure and stability of fluorescent proteins EGFP, zFP506, mRFP1, "dimer2", and DsRed1. Biochemistry (Mosc) 2004;43:14913–23.
30. Meckfessel MH, Brandt S. The structure, function, and importance of ceramides in skin and their use as therapeutic agents in skin-care products. J Am Acad Dermatol 2014;71:177–84.
31. Trommer H, Neubert RHH. Overcoming the stratum corneum: the modulation of skin penetration. A review. Skin Pharmacol Physiol 2006;19: 106–21.
32. Bole DG, Dowin R, Doriaux M, Jamieson JD. Immunocytochemical localization of BiP to the rough endoplasmic reticulum: evidence for protein sorting by selective retention. J Histochem Cytochem 1989;37: 1817–23.
33. Merad M, Sathe P, Helft J, Miller J, Mortha A. The dendritic cell lineage: ontogeny and function of dendritic cells and their subsets in the steady state and the inflamed setting. Annu Rev Immunol 2013; 31:563–604.
34. Feau S, Garcia Z, Arens R, Yagita H, Borst J, Schoenberger SP. The CD4+ T-cell help signal is transmitted from APC to CD8+ T-cells via CD27–CD70 interactions. Nat Commun 2012;3:948.
35. Ahrends T, Bąbała N, Xiao Y, Yagita H, van Eenennaam H, Borst J. CD27 agonism plus PD-1 blockade recapitulates CD4+ T-cell help in therapeutic anticancer vaccination. Cancer Res 2016;76:2921–31.
36. Ahrends T, Spanjaard A, Pilzecker B, Bąbała N, Bovens A, Xiao Y, et al. CD4+ T cell help confers a cytotoxic T cell effector program including coinhibitory receptor downregulation and increased tissue invasiveness. Immunity 2017;47:848–61.
37. Pape KA, Catron DM, Itano AA, Jenkins MK. The humoral immune response is initiated in lymph nodes by B cells that acquire soluble antigen directly in the follicles. Immunity 2007; 26:491–502.
38. Heit A, Huster KM, Schmitz F, Schiemann M, Busch DH, Wagner H. CpG-DNA aided cross-priming by cross-presenting B cells. J Immunol 2004; 172:1501–7.
39. Hon H, Oran A, Brocker T, Jacob J. B lymphocytes participate in cross-presentation of antigen following gene gun vaccination. J Immunol 2005; 174:5233–42.
40. He R, Hou S, Liu C, Zhang A, Bai Q, Han M, et al. Follicular CXCR5-expressing CD8+ T cells curtail chronic viral infection. Nature 2016; 537:412–28.
41. Lutz MB. Induction of CD4 + regulatory and polarized effector/helper T cells by dendritic cells. Immune Netw 2016;16:13.
42. Malissen B, Tamoutounour S, Henri S. The origins and functions of dendritic cells and macrophages in the skin. Nat Rev Immunol 2014;14: 417–28.
43. Kranz LM, Diken M, Haas H, Kreiter S, Loquai C, Reuter KC, et al. Systemic RNA delivery to dendritic cells exploits antiviral defence for cancer immunotherapy. Nature 2016;534:396–401.
44. Chen X, Nadiarynkh O, Plotnikov S, Campagnola PJ. Second harmonic generation microscopy for quantitative analysis of collagen fibrillar structure. Nat Protoc 2012;7:654–69.

AACR American Association for Cancer Research

Cancer Immunology Research

Subcellular Localization of Antigen in Keratinocytes Dictates Delivery of CD4 + T-cell Help for the CTL Response upon Therapeutic DNA Vaccination into the Skin

Nikolina Babala, Astrid Bovens, Evert de Vries, et al.

Cancer Immunol Res 2018;6:835-847. Published OnlineFirst May 15, 2018.